Available online at www.sciencedirect.com
SCIENCE DIRECT®
Intermetallics 12 (2004) 69–74
Intermetallics
www.elsevier.com/locate/intermet

Intermetallics in the Zr–Al diffusion zone

A. Laik, K. Bhanumurthy, G.B. Kale*

Materials Science Division, Bhabha Atomic Research Centre, Mumbai 400 085, India

Received 20 August 2003; received in revised form 2 September 2003; accepted 2 September 2003

Abstract

Solid-state diffusion reaction between Zr and Al was studied in the temperature range 838–898 K employing bulk diffusion couples. The intermetallic phase $ZrAl_3$ forms in the diffusion zone in all the diffusion couples in planar morphology. A second layer of Zr_2Al_3 forms in addition, at and above 873 K in the diffusion zone. The formation of $ZrAl_3$ as the first phase was rationalised on the basis of the Modified Effective Heat of Formation (MEHF) model. The driving forces for formation of Zr_2Al_3 and $ZrAl_2$ at the $Zr/ZrAl_3$ interface were evaluated. The appearance of Zr_2Al_3 in preference to $ZrAl_2$ at higher temperatures is attributed to the higher driving force for its formation at the $Zr/ZrAl_3$ interface. The temperature dependence of growth of $ZrAl_3$ phase layer was determined. The activation energy (Q_k) for growth of $ZrAl_3$ is 188.2±2.5 kJ/mol and the pre-exponential factor (k_0) is $2.9^{+0.55}_{-0.35} \times 10^4$ m/s$^{1/2}$.
© 2003 Elsevier Ltd. All rights reserved.

Keywords: A. Multiphase aluminides; A. Aluminides, miscellaneous; B. Diffusion; D. Phase interfaces; E. Phase stability, prediction

1. Introduction

Zirconium–aluminium alloys are potential structural materials in thermal nuclear reactors due to good mechanical properties at high temperature combined with low absorption cross-sections for thermal neutrons [1–3]. Extensive work has been reported on the Zr–Al alloys regarding amorphisation [4], nano-phase formation [5], formation of several metastable phases [6] and also making zirconium based pressure tubes with aluminium lining [7]. The Zr–Al phase diagram [8–10] shows ten intermetallic compounds (IMC) viz. Zr_3Al, Zr_2Al, Zr_5Al_3, Zr_3Al_2, Zr_4Al_3, Zr_5Al_4, ZrAl, Zr_2Al_3, $ZrAl_2$ and $ZrAl_3$. These IMC's are all essentially line compounds. Experimental reinvestigation on the Zr rich side of the Zr–Al phase diagram in the temperature range of 773–1573 K by Peruzzi [11] suggested modifications in the temperatures of some of the invariant reactions. In addition, a thermodynamic assessment of this system is reported recently [12]. Kidson and Miller [13] have studied the chemical diffusion between Zr and Al using bulk diffusion couples in the temperature range of 826–913 K for a maximum of 144 h duration mainly to develop a protective layer for zircaloy-2 pressure tube material in thermal nuclear reactors against absorption of hydrogen. They have reported the formation of only $ZrAl_3$ in the diffusion zone. Gukelberger and Steeb [14] have studied the interdiffusion between Zr and Zr_2Al_3 in the temperature range 1273–1573 K using incremental couples and reported the formation of Zr_5Al_3, Zr_3Al_2 and Zr_4Al_3 intermetallic compounds in the diffusion zone. Recently, thin film interdiffusion studies between Zr and Al showed the formation of $ZrAl_3$ at the interface [15].

The present work involves a detailed diffusion reaction study between nuclear grade pure Zr and pure Al in the temperature range 838–898 K in narrow steps of 20 K. The morphology and composition of the intermetallic phases formed by prolonged annealing at isothermal temperatures are characterised by electron probe micro-analyser (EPMA). The formation of $ZrAl_3$ as the first phase is rationalised using the modified effective heat of formation (MEHF) model. The thermodynamic basis for the formation of the second phase, Zr_2Al_3, at higher temperatures of annealing is explained.

2. Experimental procedure

Rectangular pieces of pure Zr (99.9%) and pure Al (99.9%) of approximately 10 × 5 × 4 mm^3 size were cut from rolled sheets and annealed in vacuum (better than

* Corresponding author. Tel.: +91-22-2559-5062; fax.: +91-22-2550-5239.
E-mail address: gbkale@apsara.barc.ernet.in (G.B. Kale).

0966-9795/$ - see front matter © 2003 Elsevier Ltd. All rights reserved.
doi:10.1016/j.intermet.2003.09.002

10^{-3} Pa) at 1223 K and 673 K respectively for 5 days for grain coarsening. The chemical analysis of the zirconium and aluminium used is given in Table 1. Both these samples were metallographically polished to a surface finish better than 1 μm and cleaned with acetone. In order to remove the oxide layer on Al pieces, the polished faces were mildly etched with an alkaline etchant. This cleaning was an absolutely essential step prior to bonding of Al/Zr diffusion couples. The polished and treated faces of the aluminium pieces were kept in contact with the polished faces of the zirconium pieces and were loaded in a specially made stainless steel screw type jig under a pressure of 5 MPa. Mica sheets were used as spacers on both sides of the diffusion couple to prevent contact with the stainless steel jig. The entire jig assembly was encapsulated in a quartz tube in vacuum better than 10^{-3} Pa. The evacuated quartz tube was flushed with He several times and finally sealed at a residual pressure of 2×10^4 Pa. The sealed couples were annealed isothermally in a pre-heated horizontal resistance-heating furnace while controlling the temperature within ± 1 K by a proportional temperature controller. Four such couples were made and annealed at 838 K, 858 K, 873 K and 898 K for 605 ks each. Since it has been shown in the earlier studies that the layer growth kinetics is diffusion-controlled [13], isochronal annealing was carried out in the present study to evaluate the temperature dependence of the growth of the phases and to estimate the activation energy for growth of the phases. The annealing conditions and the various phases formed in each couple are given in Table 2. The diffusion couples thus annealed were subsequently air-cooled. Annealing at temperature above 898 K was not successful due to the formation of a large gap at the Zr/Al interface, leading to detachment of the diffusion couples.

The diffusion-annealed couples were sectioned perpendicular to the bond interface with a low-speed diamond saw. These samples were mounted and the cross-sections were prepared by standard metallographic technique to a surface finish of 1 μm. Electron probe microanalysis (EPMA, CAMECA SX100) of the cross sections of the couples was carried out to obtain the concentration profiles across the diffusion zone. The entire analysis was carried out using a stabilised electron beam of 20 keV energy and 20 nA current. The standard PAP correction programme was used for atomic number (Z), absorption (A) and fluorescence (F) corrections to arrive at the true concentration from the intensity data. Pure Zr and pure Al were used as standards. Point counting technique was used to identify the phases formed in the diffusion zone. The concentration profile across the diffusion zone was determined by quantitative analysis on points at regular intervals of 1 μm. Scanning electron microscopy (SEM) was carried out on the diffusion-annealed samples in etched condition and the etchant used in these studies was H_2O:HNO_3:HF::10:9:1 by volume. The annealed couples were fractured at the interface and the fractured surfaces were analysed by X-ray diffraction to identify the intermetallic compounds formed at the diffusion zone.

Table 1
Chemical analysis (in ppm) of zirconium and aluminium used in making the diffusion couples

Elements	Fe	Si	Cu	Ca	Hf	Cr	O	C	Zr	Al
Zirconium	500	10	20	50	80	50	780	40	Balance	10
Aluminium	300	400	30	30	–	–	–	–	–	Balance

Table 2
Annealing conditions and the phases formed at the interface

Couple no.	Temperature (K)	Time (ks)	Phases formed
1	838	605	$ZrAl_3$
2	858	605	$ZrAl_3$
3	873	605	$ZrAl_3$, Zr_2Al_3
4	898	605	$ZrAl_3$, Zr_2Al_3

3. Results and discussion

3.1. Microstructure of the diffusion zone

A typical back-scattered electron (BSE) micrograph for the couple annealed at 873 K for 605 ks is shown in Fig. 1. The micrograph shows the formation of two phases in the diffusion zone. Both the phases form as layers of uniform thickness in the diffusion zone. The concentration profile taken across the diffusion zone, along a line marked A–B on Fig. 1 is shown in Fig. 2. The point count analysis at several places on the two

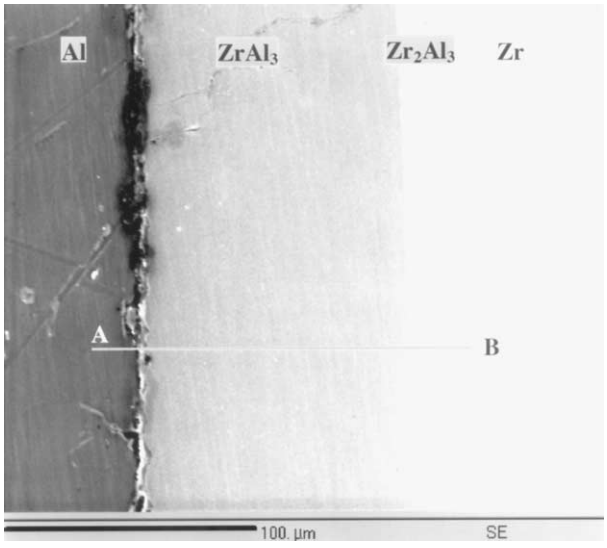

Fig. 1. BSE image of Zr–Al diffusion couple annealed at 873 K for 7 days.

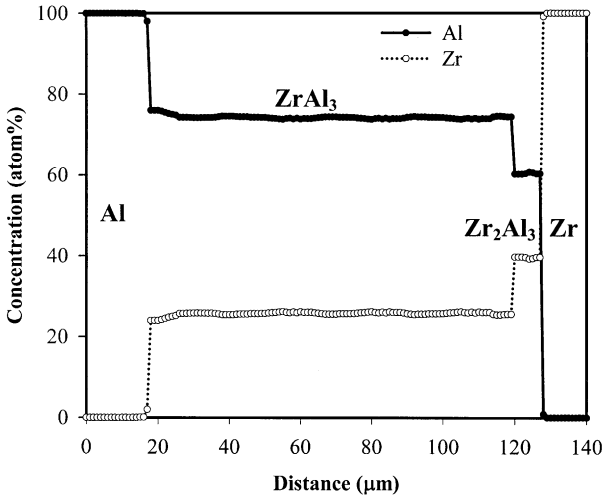

Fig. 2. Concentration profile across the diffusion zone of the diffusion couple shown in Fig. 1.

layers confirms these two phases to be Zr_2Al_3 (close to Zr) and $ZrAl_3$ (close to Al). The width of the $ZrAl_3$ layer is about an order of magnitude higher than that of Zr_2Al_3. The diffusion couple annealed at 898 K for 605 ks has also revealed only two phases i.e. Zr_2Al_3 and $ZrAl_3$. However, the diffusion couples annealed at lower temperatures, i.e. 838 K and 858 K for 605 ks, showed only one phase, $ZrAl_3$. High-resolution secondary electron micrographs of $Zr_2Al_3/ZrAl_3$, $Zr/ZrAl_3$ and Zr/Zr_2Al_3 interfaces showed them to be continuous and free from any porosity or discontinuities for all the couples. However, the $ZrAl_3$/Al interface for all the couples showed porosity and voids. The weak bonding at $ZrAl_3$/Al could be due to: (a) large difference in the thermal coefficient of expansion between Al ($\alpha = 21.3 \times 10^{-6}$ K^{-1} at 293 K) and Zr ($\alpha = 5.5 \times 10^{-6}$ K^{-1} at 293 K) and/or (b) a pronounced Kirkendall effect arising from the large difference in the diffusivity of Al and Zr.

Kidson and Miller [13] have indicated the formation of only $ZrAl_3$ phase for all the couples annealed between 826 and 913 K for time intervals up to 518 ks. The present experiment clearly shows the presence of a layer of Zr_2Al_3 along with the thick layer of $ZrAl_3$ in the diffusion zone of the couples annealed at temperatures at and above 873 K.

Both the phases formed are uniform in width and their interfaces are nearly parallel to the original interface. The average compositions of the phases as measured at the interfaces by microprobe analysis in the present study and those reported in the equilibrium diagram [8] are listed in Table 3. It can be seen that the compositions of $ZrAl_3$ and Al(Zr) do not differ significantly from those depicted by the equilibrium phase diagram. However, there is a small difference in the composition of the solid solution of Zr(Al) and Zr_2Al_3. This possibly is due to the absence of the intermediate phases between Zr_2Al_3 and Zr. It may be inferred that the composition of the various phase boundaries reach near equilibrium values only when the adjacent phases form in the diffusion zone. The attainment of near equilibrium compositions of the coexisting phases in multi-phase diffusion couples has been reported earlier [16].

3.2. Formation of phases in the diffusion zone

3.2.1. Formation of $ZrAl_3$

The Zr–Al phase diagram indicates the presence of Zr_3Al, Zr_2Al, Zr_3Al_2, Zr_4Al_3, ZrAl, Zr_2Al_3, $ZrAl_2$, and $ZrAl_3$ in the temperature range of the present study, of which only Zr_2Al_3 and $ZrAl_3$ were found to form within the diffusion zone. Amongst these equilibrium phases, Zr_2Al_3 has the most negative free energy of formation. Therefore, thermodynamically it is expected to form first at the Zr–Al interface during the process of annealing. But not only energetics but kinetics are equally important in deciding the nucleation and growth of a particular phase. In the present case of the Zr–Al system, although thermo-dynamically Zr_2Al_3 is more favourable, experimental observations show that $ZrAl_3$ forms first at the Zr–Al interface. The formation of a phase in the diffusion zone involves a series of events like formation of saturated primary solid solutions, nucleation of an intermediate phase and finally the growth of the nucleated phase. Only when the conditions for all the events are favourable may a particular phase appear at the interface. In the present case of the Zr–Al system, saturated solid solutions of α-Zr(Al) and Al(Zr) form on the either side due to interdiffusion. It is to be noted that the solubility limit of Al in Zr is ~1.2 at.% in the temperature range studied, i.e. 838–898 K, whereas the maximum solubility limit of Zr in Al in the same temperature range is only 0.07 at.% [8]. Since the solubility limit of Zr in Al is an order of magnitude less, one would expect the Al(Zr) solid solution to saturate first and result in nucleation of $ZrAl_3$, as is experimentally observed.

In fact, the ease of nucleation of $ZrAl_3$ was explained by Kidson and Miller [13] in terms of the similarities in the structures of the lattices of Al(Zr) and $ZrAl_3$. It can be shown that a slightly distorted modification of the FCC lattice of Al is required to nucleate the DO_{23} type lattice of $ZrAl_3$. The interatomic spacing between near-neighbour Al–Al atoms is 2.86 Å for FCC lattice of Al, whereas the DO_{23} lattice of $ZrAl_3$ has two types of Al–Al bonds with interatomic spacings 2.80 Å and 2.85 Å. Therefore, the Zr atoms on diffusing in the Al matrix occupy the ordered arrangement sites and hence nucleate the $ZrAl_3$ phase without generation of any significant misfit energy.

A good number of models exist in the literature on prediction of the formation of the first phase [17–22]. Amongst these, the effective heat of formation (EHF)

Table 3
Composition (in at.%) of the phases formed in the diffusion zone

Temperature (K)	Conc. of Zr in phases observed in the diffusion zone							
	Zr(Al)		Zr_2Al_3		$ZrAl_3$		Al(Zr)	
	PD	DC	PD	DC	PD	DC	PD	DC
873	99.5	98.6	40	39.66	25	25.4	0.07	0.07
898	99.5	98.2	40	39.60	25	25.6	0.08	0.08

PD = phase diagram; DC = diffusion couple.

model proposed by Pretorius [21,22] is the most recent and is successful in predicting the first phase of formation in many binary systems such as M–Al and M–Ge (M = metal). The EHF model combines the thermodynamic data with the concentrations of the reacting species at the growth interface. Based on this model, the effective heat of formation (EHF), $\Delta H'$, is defined as:

$$\Delta H' = \Delta H^0 \frac{C_e}{C_l} \tag{1}$$

where, ΔH^0 is the standard heat of formation, C_e is the effective concentration of the limiting element at the interface, taken as the composition of the limiting element at the lowest liquidus temperature, and C_l is the concentration of the limiting element in the compound.

However, Pretorius' EHF model [21,22] has difficulty in predicting the first phase in some systems where congruent and non-congruent compounds are simultaneously present. Bhanumurthy et al. [23] had proposed a modification to the EHF model by incorporating a congruency factor, ΔH^f, and defined the modified effective heat of formation (MEHF) as:

$$\Delta H^m = \left(\Delta H^0 + \Delta H^f\right)\frac{C_e}{C_l} \tag{2}$$

Here ΔH^f is assumed to be equal to the heat of crystallisation of the compound for congruent compounds and zero for non-congruent compounds formed at the interface. The congruency factor can be empirically related to the melting point T_m of the intermediate phase by [23]:

$$\Delta H^f = 8.13\ \ T_m\ \ \text{J/mol} \tag{3}$$

On the basis of this model, the values of ΔH^m have been calculated for all the com-pounds appearing in the phase diagram in the temperature range of present study and are listed in Table 4 along with the values of ΔH^0. It can be seen from the table that $ZrAl_3$ has the maximum negative modified effective heat of formation (ΔH^m) and hence this phase is expected to form first at the diffusion zone. In fact, this phase is observed experimentally in all the couples annealed in the present study.

3.2.2. Formation of Zr_2Al_3

The next phase to appear in the diffusion zone is Zr_2Al_3. It needs to be mentioned that the presence of the equilibrium phase $ZrAl_2$ could not be detected in the diffusion zone in the present experiments. The possible reason for absence of the phase can be explained considering the thermodynamics of the α-Zr(Al)/$ZrAl_3$ interface.

The free energy for a solid-solution phase P in a binary system A–B can be represented mathematically as [24,25]:

$$G^P = x_A G_A^P + x_B G_B^P + G_{mix}^{xs} - TS_{mix}^{id} \tag{4}$$

where, x_A and x_B are the mole fractions of the elements A and B respectively, G_A^P and G_B^P are the lattice stabilities of the elements A and B respectively in the phase P, $S_{mix}^{id}(= -R[x_A \ln x_A + x_A \ln x_A])$ is the ideal entropy of mixing, and T is the absolute temperature. G_{mix}^{xs}, the excess free energy of mixing for the phase P, can be expressed mathematically by the relation:

$$G_{mix}^{xs} = x_A x_B \sum_{j=0}^{m} \left(a_j + a_j' T\right)(x_A - x_B)^j \tag{5}$$

For a regular solution $m = 0$, for a sub-regular solution $m = 1$ and for a real solution the value of m is greater than 1 but generally does not exceed 2 [26]. a_j and a_j' are the parameters of the phase P. In our calculations we take $m = 2$, assuming the system to be a real solution. The values of the parameters a_j and a_j' for the α-Zr(Al) solid solution phase and G_{Al}^{hcp} and G_{Zr}^{hcp} (the lattice stabilities of Al and Zr in the hcp lattice of the α-Zr(Al) solid-solution phase) used in the present calculations are taken from the literature [27]. The Gibbs free energy-composition diagrams at temperature 873 K were plotted for α-Zr solid solution, $ZrAl_3$, $ZrAl_2$ and $Zr2Al_3$ compounds as shown in Fig. 3. (As the intermediate compounds in Zr–Al are all stoichiometric line compounds, the solubility range of these compounds shown in Fig. 3 are not truly representative, but are exaggerated to enhance clarity of the diagram). Assuming local equilibrium between α-Zr solid solution and $ZrAl_3$, we draw a common tangent between the two curves. The driving force for formation of $ZrAl_2$ and Zr_2Al_3 at the Zr/$ZrAl_3$ interface are ΔG_{ZrAl_2} and

Table 4
The values of ΔH^0 and ΔH^m, for the various intermediate phases in the Zr–Al system

Phase	Congruent/noncongruent	Limiting element	ΔH^0 (kJ/mol at)	ΔH^m (kJ/mol at)
Zr_3Al	NC	Zr	−28.7	−0.89
Zr_2Al	NC	Zr	−36.3	−1.28
Zr_3Al_2	NC	Zr	−41	−1.37
Zr_4Al_3	NC	Zr	−43	−1.51
ZrAl	NC	Zr	−45	−1.8
Zr_2Al_3	NC	Zr	−47	−2.35
$ZrAl_2$	C	Zr	−46	−3.69
$ZrAl_3$	C	Zr	−41	−4.48

C = congruent; NC = non-congruent.

$\Delta G_{Zr_2Al_3}$ respectively as shown in Fig. 3. It is clear that the value of $\Delta G_{Zr_2Al_3} = -10.77$ kJ/mol is more negative than that of $\Delta G_{ZrAl_3} = -7.18$ kJ/mol at 873 K. The higher driving force for Zr_2Al_3 may have led to the formation of Zr_2Al_3 in preference to $ZrAl_2$ phase at the Zr/$ZrAl_3$ interface. The present experiments confirm that the dominant phase in the diffusion zone is $ZrAl_3$ and occupies almost 90% of the diffusion zone at 873 K and above. This substantial growth may be due to relatively large diffusion coefficient of Zr and Al in this phase. Assuming the diffusion coefficient, $D = \frac{x^2}{2t}$, where x is the width of the phase and t is the time duration for annealing, D for $ZrAl_3$ is 10^{-14} m^2/s. This rapid diffusion of Zr and Al in this phase may be primarily responsible for the exclusion of other phases in the diffusion zone.

3.3. Kinetics of layer growth

An earlier study showed that the growth of the $ZrAl_3$ phase layer is parabolic with respect to time, i.e., a diffusion-controlled process [13]. The width of the phase, w, can be represented by:

$$w = k\sqrt{t} \tag{6}$$

where, t is the time of annealing and k is the rate constant. For an isochronal type of annealing, the width of the phase can be related to the temperature of annealing, T, by a simple Arrhenius type of relation:

$$w = k_0\sqrt{t}\exp\left(\frac{-Q_k}{RT}\right) \tag{7}$$

where, t is the time of annealing, k_0 and Q_k are the pre-exponential factor and activation energy for growth of $ZrAl_3$ respectively.

The logarithmic values of the widths of the $ZrAl_3$ layer were plotted against $1/T$ as shown in Fig. 4. A straight line was fitted to the data points by the least square method. The values of Q_k and k_0 were determined from the slope and intercept of the plot. The values of Q_k and k_0 are 188.2±2.5 kJ/mol and $2.9^{+0.55}_{-0.35} \times 10^4$ $m/s^{1/2}$ respectively. The values of Q_k and k_0 reported by Kidson and Miller [13] are 192.28 kJ/mol and 3.70×10^5 $m/s^{1/2}$ respectively. The activation

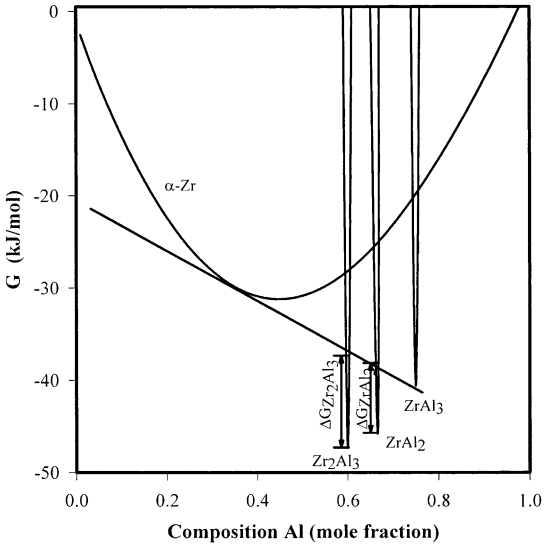

Fig. 3. Free energy (G) versus composition (x) plot of the Zr–Al system at 873 K.

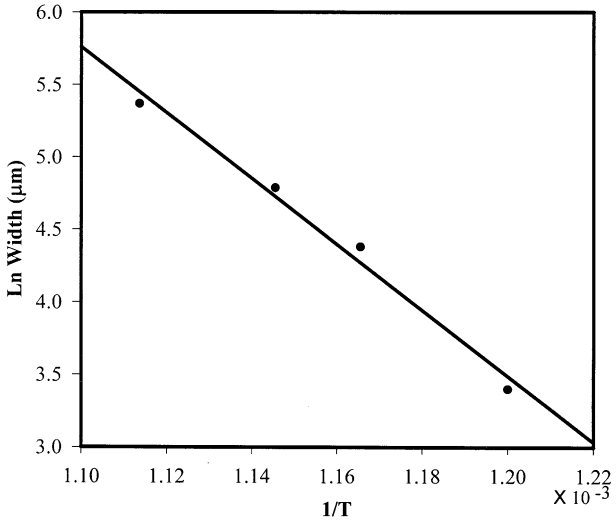

Fig. 4. Temperature dependence of the growth of $ZrAl_3$ layer.

energy (Q_k) estimated from the present investigation, matches well with the earlier reported values [13].

4. Conclusions

The present study on bulk diffusion couples of Zr/Al confirms the formation of $ZrAl_3$ phase in a planar morphology on annealing the couple in the temperature range 838–898 K. The modified effective heat of formation (MEHF) model explains the appearance of $ZrAl_3$ as the first phase in the diffusion zone. Annealing at temperatures 873 K and above results in formation of an additional layer of Zr_2Al_3 phase at the $Zr/ZrAl_3$ interface. The formation of Zr_2Al_3 in preference to $ZrAl_2$ can be attributed to higher driving force for formation. The appearance for pores and void at the $Al/ZrAl_3$ interface may be due to the difference in the intrinsic diffusivities of Zr and Al and hence is a manifestation of Kirkendall effect. The temperature dependence of growth of the $ZrAl_3$ layer can be described by an Arrhenius relation with an activation energy (Q_k) of 188.2 ± 2.5 kJ/mol and a pre-exponential factor (k_0) of $2.9^{+0.55}_{-0.35} \times 10^4$ m/s$^{1/2}$.

Acknowledgements

The authors wish to express their gratitude to Dr P.K. De, Head, Materials Science Division and Dr S. Banerjee, Director, Materials Group, BARC for their constant sup-port. The help extended by Mr P.S. Gawde in carrying out the experiments is gratefully acknowledged.

References

[1] Schulson EM. In: Westbrook JH, Fleischer RL, editors. Intermetallic compounds, vol. 2. John Wiley and Sons; 1994. p. 133.
[2] Cox B. Report no. AECL-2776. Canada: Atomic Energy of Canada Limited; 1967.
[3] Ibrahim EF, Cheadle BA. Can Metall Q 1985;24(3):273.
[4] Sheng HW, Lu K, Ma E. J Appl Phy 1999;85:6400.
[5] Fu Z, Jonson WL. Nanostructured Materials 1993;3:175.
[6] Gialanella S, Yavari AR, Cahn RW. Scripta Metall Mater 1992; 26:1233.
[7] Schulson EM, Stewart MJ. Metall Trans B 1976;7B:363.
[8] Peruzzi A, Abraita JP. In: Massalski TB, editor. Alloy binary alloy phase diagrams. 2nd ed. OH: ASM International; 1990. p. 241.
[9] Murray Z, Peruzzi A, Abraita JP. J Phase Equil 1992;13:277.
[10] Okamoto H. J Phase Equil 1993;14:259.
[11] Peruzzi A. J Nucl Mater 1992;186:89.
[12] Wang T, Jin Z, Zhao JC. J Phase Equil 2001;22:544.
[13] Kidson GV, Miller GD. J Nucl Mater 1964;1(12):61.
[14] Gukelberger A, Steeb S. Z Metallkd 1978;69:255.
[15] Pretorius R, Marais TK, Theron CC. Mat Sci Eng 1993;10:1.
[16] Romig Jr AD. Bull Alloy Phase Diag 1987;8:308.
[17] Walser RM, Bené RW. Appl Phys Lett 1976;28:624.
[18] Tsaur BY, Lau SS, Mayer JW, Nicolet MA. Appl Phys Lett 1981; 38:922.
[19] Bené RW. Appl Phys Lett 1982;41:529.
[20] Ronay M. Appl Phys Lett 1983;42:577.
[21] Pretorius R. MRS Proc 1984;25:15.
[22] Pretorius R, de Reus R, Vredenberg AM, Saris FW. J Appl Phys 1991;70:3636.
[23] Bhanumurthy K, Kale GB, Garg SP. Trans Indian Inst Met 1995; 48:193.
[24] Kaufman L, Bernstein H. In: Computer calculation of phase diagrams. New York: Academy Press; 1970.
[25] Kubaschewski O, Chart TG. J Inst Met 1965;93:329.
[26] Saunders N, Miodownik AP. In: Calphad—calculation of phase diagrams- a comprehensive guide. Pergamon; 1998.
[27] Saunders N, Rivlin VG. Mat Sci Tech 1986;2:521.